

# Post-Flight Finite Element Analysis of HIFiRE-1 Aerothermal Data

Thomas H. Squire

*NASA Ames Research Center, Moffett Field, CA 94035-0001*

Parul Agrawal and Dinesh Prabhu

*ERC Inc., Moffett Field, CA 94035-0001*

The Hypersonic International Flight Research and Experimentation (HIFiRE) program is a joint effort of the Australian Defence Science and Technology Organisation (DSTO) and the U.S. Air Force Research Laboratory (AFRL), with support from NASA, commercial space companies, and academia. The goal of the program is to investigate fundamental hypersonic flight phenomena, such as boundary layer transition and shock/boundary layer interactions. The program includes flight tests of heavily-instrumented ballistic vehicles to gather high-fidelity, aerothermal data. In March 2010, HIFiRE-1 was successfully flown in the Woomera test range in Australia. The vehicle was instrumented with nearly 200 thermocouples on the surface, as well as other sensors. In this work thermocouple temperature data from the flight were used as boundary conditions in finite element analyses of the vehicle in an inverse method to estimate of the actual heat flux experienced during the ascent portion of the flight. The analysis approach was validated using simple 1-D models of the vehicle structure. Two-dimensional axisymmetric analyses were then performed in order to quantify and account for multi-dimensional conduction effects that may exists in the measured temperature data. The heat flux distributions calculated from flight data show remarkably good agreement with CFD predications and appear to validate the turbulent transition model used in the CFD analyses.

## Nomenclature

$c_p$	specific heat	$q_{total}$	heat flux to the surface
$h$	convective transfer coefficient, of the form $q=h(T_\infty - T_w)$	$t$	time
$k$	thermal conductivity	$z$	surface depth location
$q_{cat}$	surface heat flux due to catalytic effects	$Re_\theta$	momentum thickness Reynolds number
$q_{cond}$	conduction heat flux into the structure	$T$	temperature
$q_{conv}$	convective heat flux to the surface	$T_w$	wall temperature
$q_{rad\_in}$	radiative heat flux to the surface	$T_\infty$	environment sink temperature
$q_{rad\_out}$	re-radiation heat flux from the surface	$\epsilon_w$	surface emissivity
		$\sigma$	Stefan-Boltzmann constant

## I. Introduction

The Hypersonic International Flight Research and Experimentation (HIFiRE) program is a joint effort of the Australian Defence Science and Technology Organisation (DSTO) and the U.S. Air Force Research Laboratory (AFRL).<sup>1</sup> The program is supported by NASA, commercial space companies, such as Boeing and ATK-GASL, and academia. The goal of the program is to investigate fundamental hypersonic phenomena, including boundary layer transition and shock/boundary layer interactions, develop technologies pervasive to high speed weapons, and validate phenomena and technologies at flight conditions that are difficult, if not impossible, to replicate in ground test. The program's approach is to identify key hypersonic flight issues, characterize the associated phenomena with simulations and ground tests, and then validate the predictions with flight experiments under the appropriate environmental conditions.

The first operational flight experiment of the program, HIFiRE-1, was conducted in 2010. The payload vehicle was designed to include several hypersonic flow experiments, including boundary layer transition (BLT) and

shock/boundary layer interaction (SBLI) experiments.<sup>2,3</sup> Data gathered by the onboard instrumentation are being used to validate computational fluid dynamics (CFD) predictions of the hypersonic aerothermal environment<sup>4,5,6</sup> and provide comparison with ground test experiments.<sup>7,8</sup> In order to perform these comparisons, it is necessary to accurately extract the surface heat flux on the flight test vehicle from the instrumentation data. Over 100 thermocouples (TCs) measured the surface and interior temperature response of the vehicle's metallic structure during the entire flight.

In this work, we used the measured temperature data as boundary conditions in a series of transient thermal finite element analyses (FEA) of the flight vehicle to estimate the surface heat flux history. Our analysis focused on the first 45 seconds of the ascent portion of the flight, during which the vehicle is endoatmospheric. In the following sections we provide a brief summary of the HIFiRE-1 flight experiment and data, describe the analysis objectives, approach, and results, and compare the calculate heat flux from the flight data with CFD predictions. The study of the HIFiRE-1 data is still ongoing and the work reported here represents the current status of the study.

## II. HIFiRE-1 Flight Experiment

The HIFiRE-1 flight experiment was conducted on March 22, 2010 at the Woomera Test Range in South Australia. The test vehicle was designed to incorporate both a BLT and a SBLI experiment. The test vehicle was approximately 2.1m in length (Fig. 1) and consisted of a 1.1m-long sphere-cone section with a 2.5mm radius nose tip and 7° half-angle, followed by cylindrical section, and then a 33° flare. The nose section was comprised of three components: a titanium-zirconium-molybdenum (TZM) nose tip, an AISI 1020 steel isolator, and an AISI 304 steel joiner connecting the nose assembly to the cone (Fig. 2). The cone and cylinder sections were constructed of Al 6061-T6 aluminum. The cone outer structure had a nominal shell thickness of 20mm and the cylinder was 5mm thick. The flare section was AISI 1020 with a thickness of 12mm.

- ~2.1m total length
- 2.5mm radius nose
- 0.355m base diameter

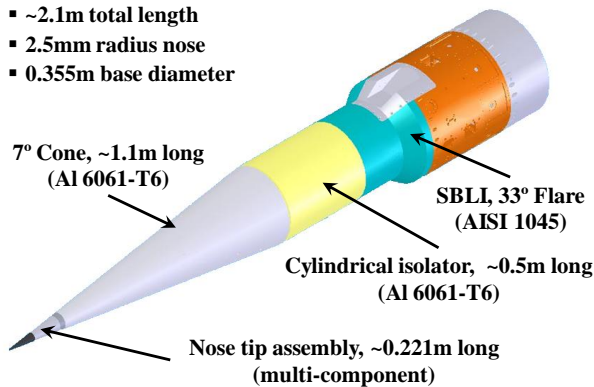


Figure 1. HIFiRE-1 flight vehicle.

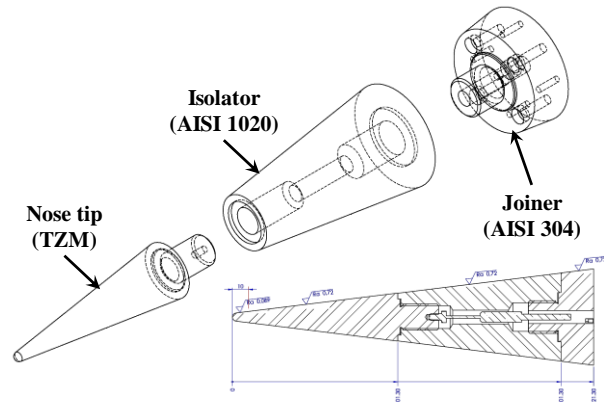
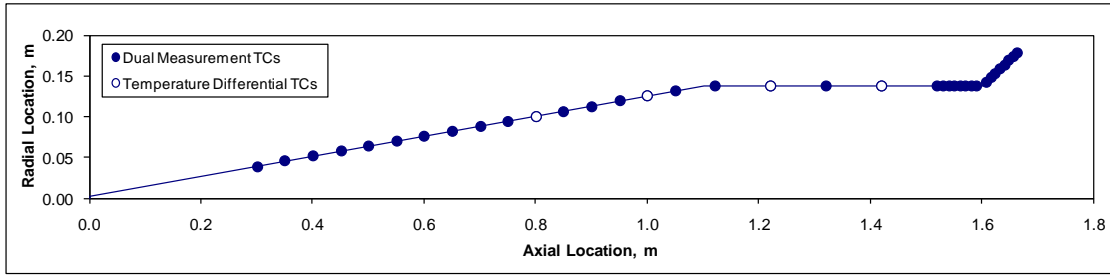


Figure 2. Nose tip assembly.

The vehicle was instrumented with 84 dual-junction Medtherm coaxial thermocouples (TCs) that independently measured both the outer and inner surface temperatures of the structure. Type T (copper-constantan) thermocouples were installed in the aluminum sections of the vehicle (cone and cylinder) and Type E (chromel-constantan) were installed on the steel sections (flare). The TCs were mounted flush with the outer and inner surfaces of the structure. An additional 24 TCs measured the temperature difference between the outer and inner surface. The post-processing of the data from the 24 differential TCs was not completed at the time this study was conducted, so they were not used in the analysis. Most of the TCs were located along two axial rays positioned 180° apart, azimuthally. The TCs were distributed along the cone, cylinder and flare sections (Fig. 3). Two internal TCs were located in the nose assembly, near the centerline of the vehicle. The instrumentation also included 68 pressure sensors and 8 direct heat transfer measurement sensors. The data from the pressure and heat transfer sensors were not used in this analysis.



**Figure 3. HIFiRE-1 TC locations along the 0° and 180° rays. (not to scale)**

The vehicle was launched on a two-stage rocket (Fig. 4) with a nominal trajectory shown in Figure 5. Several tracking stations recorded the telemetry from the vehicle during flight. A total of over 15GB of sensor data were collected along the entire trajectory before the vehicle impacted the ground. Some noise and signal drop outs were observed in the data. Of the 168 independent temperature measurements from the coaxial TCs approximately 25 failed to produce any useful data.

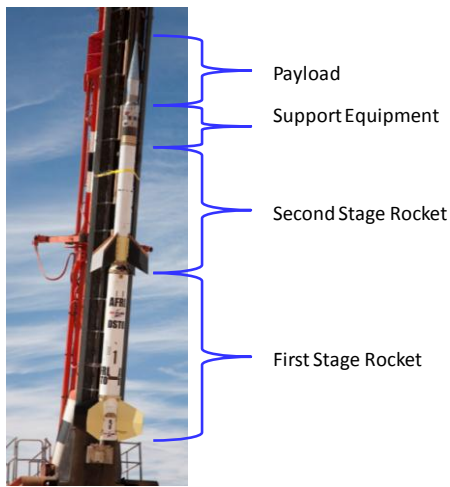


**Figure 4. Launch vehicle stack up.**

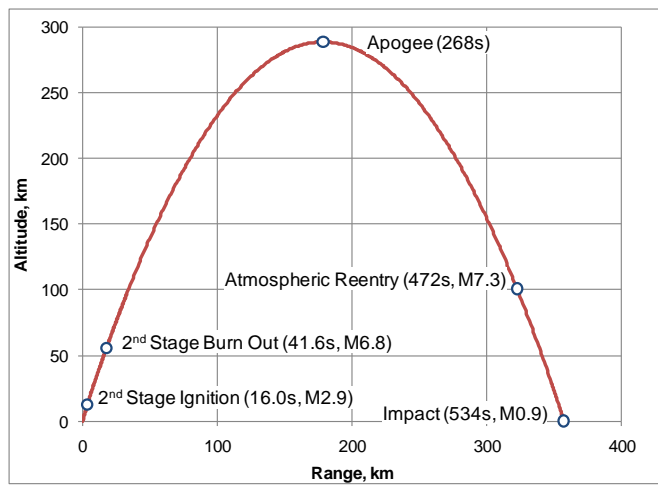


**Figure 5. Nominal HIFiRE-1 trajectory.**

### III. Finite Element Thermal Analysis Development

A variety of efforts are underway to analyze the flight data from HIFiRE-1, including an effort lead by AFRL to reconstruct the aerothermal environment on the vehicle from the thermocouple data.<sup>6</sup> The goal of this work was to compliment the AFRL effort and apply a finite element technique to analyze the data and estimate the convective heating conditions on the vehicle. This work was conducted as part of the Hypersonics Project under the NASA Fundamental Aeronautics Program.

The focus of the investigation reported here was on the analysis of the flight conditions on the conic section of the vehicle for the first 45 seconds of the flight experiment, during which the vehicle was accelerating through the atmosphere. This portion of the flight includes the ignition and burn out of the first stage rocket motor at 0.0 and 6.23 seconds, respectively, and the ignition and burn out of the second stage rocket motor at 16.0 and 41.6 seconds, respectively (Fig. 6). At 45.0 seconds the experiment payload was estimated to be at an altitude of 62.5 km and traveling a Mach 6.9 (Fig. 7). Our ultimate objective is to analyze the flight data over the entire atmospheric portion of the trajectory, including the reentry. However, the first set of analyses focused on the ascent phase, because it offered some advantages. First, preliminary examination of the thermocouple data has already been performed by AFRL using 1D thermal analysis, which provided an opportunity to validate our approach and results. Second, the recorded temperature measurements has less noise and fewer data drop outs during the early ascent portion of the trajectory than did other portions, so we had to do less pre-processing of the data sets. Finally, preliminary evaluation of the flight data indicates that the orientation of the vehicle was always 0° +/- 0.5° angle of attack (AOA) during the ascent phase and that meant that we did not have to account for large azimuthal variations in the aerothermal conditions and temperature response due to large angles of attack. Some azimuthal variation of the surface heating was expected due to the presence of boundary layer trips on some portions of the vehicle.

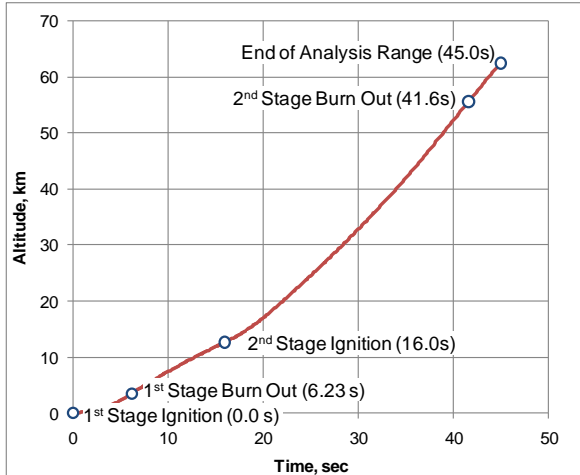


Figure 6. Analysis portion of nominal trajectory.

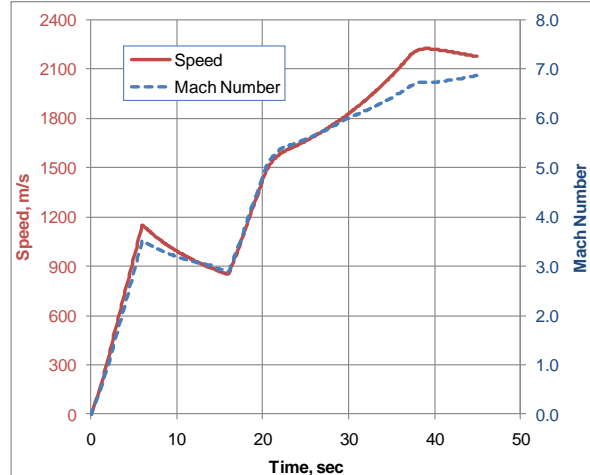


Figure 7. Speed and Mach number.

### A. Thermal Analysis Objectives and Approach

The primary objective of this work was to use the measured flight data in a transient thermal analysis to predict the temperature distribution throughout the structure and calculate the corresponding surface heat transfer rates using an inverse method. We then used those results to assess the magnitude of any multi-dimensional conduction effects on the effective heat transfer, due to structural design features and differences in material thermal properties between vehicle segments. The results were also used to estimate the internal thermal conditions of the vehicle and the heat flux predictions were compared with those from CFD analyses.

The thermal analysis of the flight TC data began with simple 1D transient thermal models and then progressed to 2D axisymmetric models. All of the thermal analyses were performed using the MSC.Marc commercial finite element analysis (FEA) package.<sup>9</sup> MSC.Marc supports fully transient, non-linear, thermal FEA. MSC.Marc can use non-linear and temperature dependent material properties. It includes an integrated user interface, Mentat, for pre- and post-processing (Fig. 8). The package allows the application of a wide range of thermal boundary conditions, such as applied heat flux, convective heating, fixed temperature, and radiation. The boundary conditions can be simple constant values or they can vary both spatially and temporally. A set of predefined user-accessible subroutines allows for a wide variety of customized control of the analysis and output. The analysis output from Marc includes the temperature gradients and reaction heat flux values at the surface boundaries, which were the primary quantities of interest in our analysis.

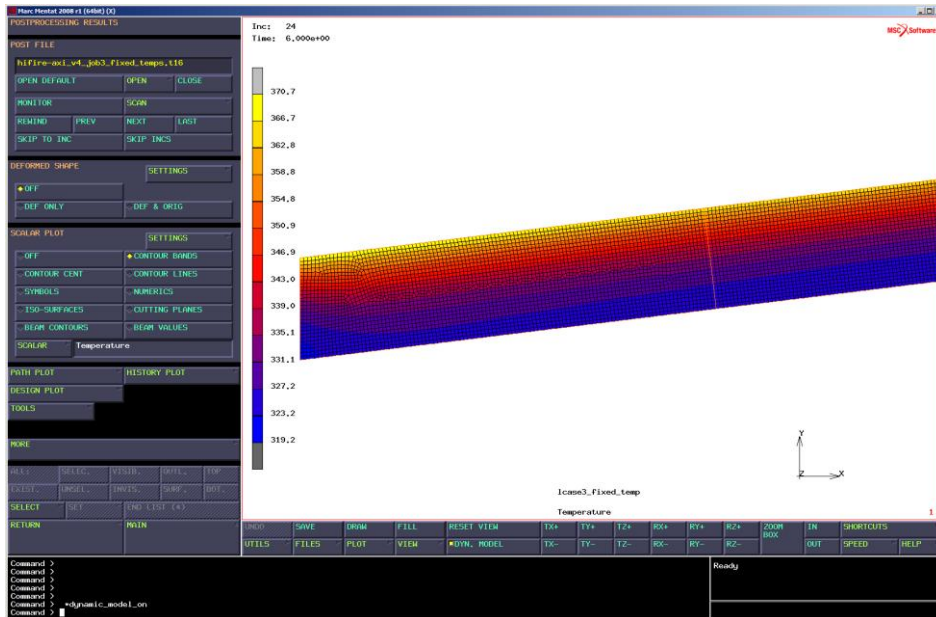
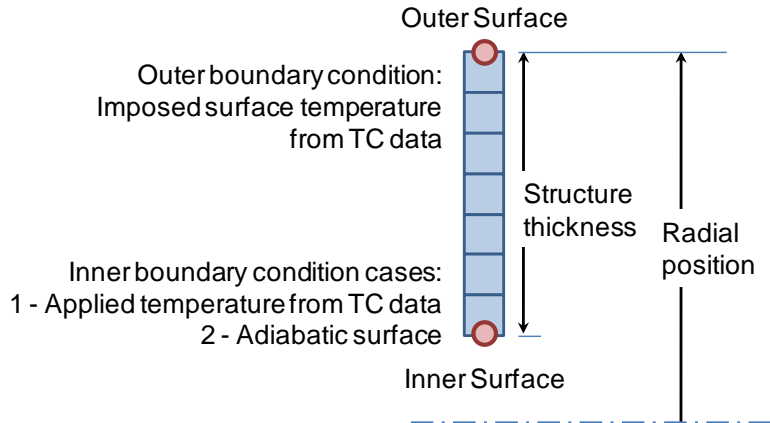


Figure 8. Marc/Mentat user interface.

### B. Finite Element Model Design

Both 1D and 2D finite element models of the conic section of the HIFiRE vehicle were constructed and analyzed. The 1D model consisted of arrays of elements through the thickness of the cone structure and normal to the surface at the locations of the dual-junction TCs. A notional image of the models is shown in Figure 9. The mesh included 100 elements through the thickness of the cone. The elements used quadratic interpolation functions. In order to account for the cylindrical nature of the vehicle, the 1D model used axisymmetric elements and the outer surface was located at radial position corresponding to the position of the TC on the cone.



**Figure 9. Notional 1D FEA model.**

The 2D FEA model included an axisymmetric cross section of the entire test vehicle (Fig 10). The model was constructed of 8-noded quadrilateral elements using bi-quadratic interpolation functions. The average element size was nominally 0.75 mm on a side. The aluminum conic section, which is the focus of this work, had approximately 30 elements through the thickness of the structure, which was 20 mm thick, and the cone section consisted of about 33,500 elements. The entire cross section model consisted of about 48,600 elements. Each of the individual segments of the model was assumed to be in perfect thermal contact.

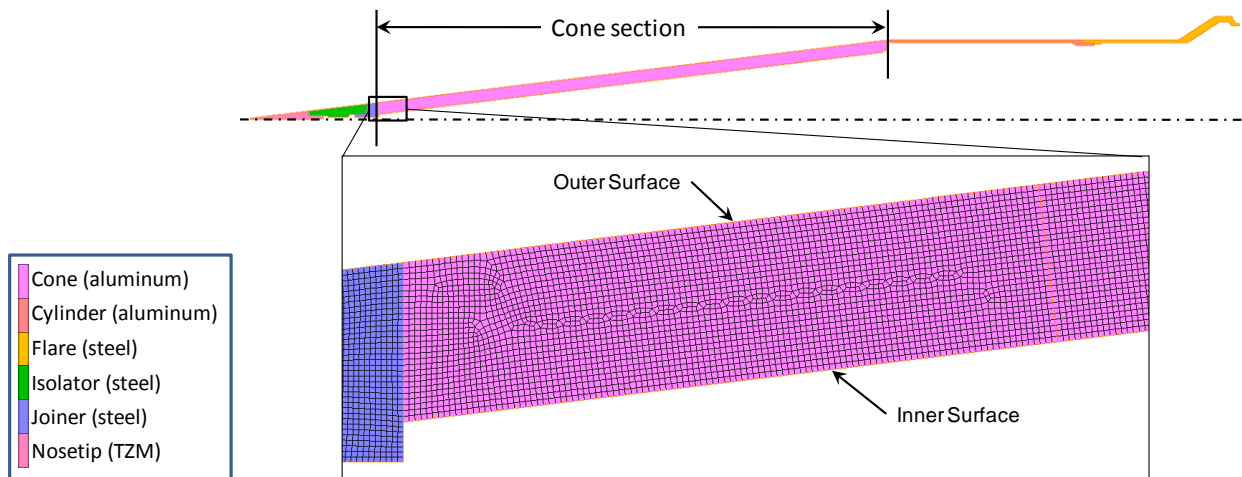


**Figure 10. 2D FEA model and mesh.**

Both the 1D and 2D FEA models used Al 6061-T6 material properties for the analysis of the cone section of the vehicle, with a density of  $2700 \text{ kg/m}^3$  and temperature-dependent thermal conductivity and specific heat (Table 1). In the 2D model the cone section is attached to an AISI 304 steel "joiner" at the forward end and an aluminum cylinder section at the aft end. The AISI 304 had a density of  $7752 \text{ kg/m}^3$  and other thermal properties as shown in Table 1.

**Table 1. Analysis Thermal Properties**

Al 6061-T6			AISI 304 Steel		
Temp (C)	$c_p$ (J/kg-K)	$k$ (W/m-K)	Temp (C)	$c_p$ (J/kg-K)	$k$ (W/m-K)
-273.0	0.0	8.6	-273.0	242.8	0.31
-184.1	502.4	66.0	-17.4	242.8	13.3
-128.6	682.4	93.5	204.8	460.5	16.3
-17.4	879.2	117.8	427.0	669.9	19.2
93.7	963.0	133.3	538.1	745.3	20.8
315.9	1067.6	150.0	649.2	703.4	21.8
427.0	1130.4	154.0	871.4	552.7	25.2
5282.6	1130.4	154.0	5282.6	552.7	31.8

**C. Boundary and Initial Conditions**

The outer surface temperature boundary condition was set to the actual measured temperature histories from the TC flight data. On the inner (interior) surface two different boundary condition cases were considered: the first case set the temperature to the measured TC data from the inner surface; the second case used an adiabatic (insulated) condition. For the 2D axisymmetric analyses the temperature between each TC location was assumed to vary linearly with streamlength (Fig. 11). The adiabatic inner surface boundary condition allowed us to compare the predicted inner surface temperature with the measured temperature from the TC data and assess just how accurate an adiabatic inner surface boundary condition was for the actual flight vehicle. Future 3D finite element analyses of the HIFiRE-1 flight data will be greatly simplified if an adiabatic inner surface boundary condition can be used instead of a prescribed temperature history. The initial temperature of the entire vehicle was set to a constant value equal to the average of the measured TC temperatures at  $t=0$ , which was 37C.

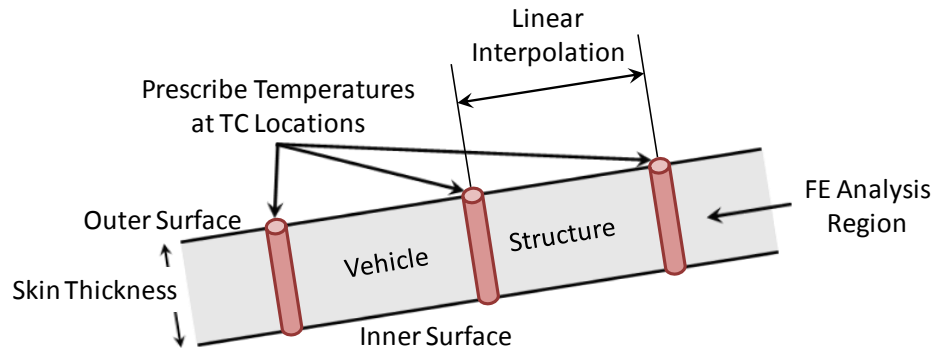


**Figure 11. 2D FEA boundary condition schematic.**

**D. Thermocouple Data Used in Thermal Analysis**

The 1D and 2D axisymmetric analyses were performed with the data taken from the series of TCs located along the 0° azimuthal ray of the cone section of the HIFiRE-1 vehicle (Fig. 12). The array consisted of sixteen TCs, four of which failed during the flight. All of the dual-junction TCs were designated with a unique number. The 1D analyses focused on three of the sixteen TC pair locations: the one furthest forward on the cone, the one furthest back, and one near the middle, designated as TC 4/3, TC 31/32, and TC 21/22, respectively. The first number in the designation indicates the outer surface junction and the second the inner surface junction. The two TCs 4/3 and 31/32 were chosen for analysis because they were located closest to the ends of the cone and were most likely to show effects of multi-dimensional conduction due their proximity to the interfaces with other vehicle sections. TC 21/22 was chosen because it was near the center of the cone, which was more likely to exhibit 1D conduction behavior.

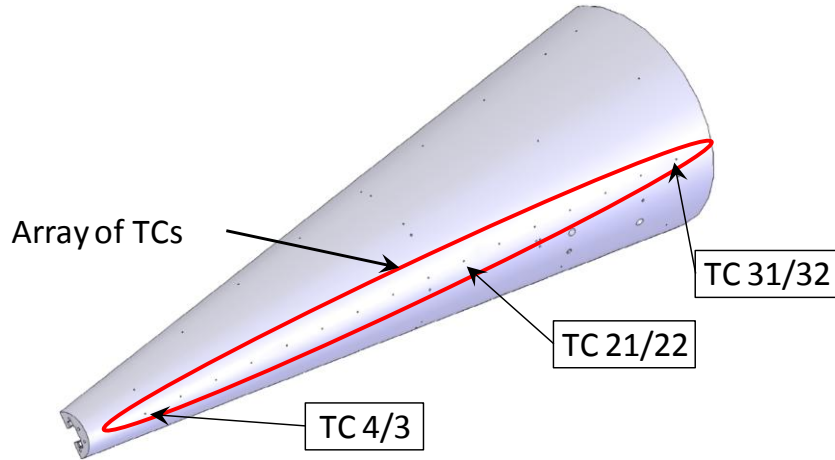


**Figure 12. TC array on the conic section.**

The TC data were sampled at a rate of 400 Hz during the flight, which resulted in large data sets. In order to reduce the size of the data sets used in the analysis, we chose to resample the data at every 0.1 sec time step (10 Hz). The reduced TC data temperature history for TC 4/3, TC 21/22, and TC 31/32 is shown in Figures 13, 14, and 15, respectively. Note that there are still some data drop outs still visible in the data sets. These drop outs were manually identified and removed before being used in the analysis. The bad data points were simply removed from the data set and effectively replaced by a linear interpolation between the data points immediately prior and after the removed point. Some noise still appears in the reduced data sets, but no effort was made to remove it.

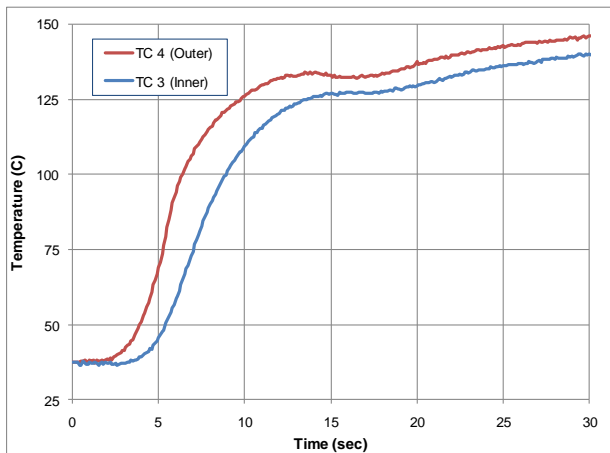


**Figure 13. TC 4/3 temperature data.**

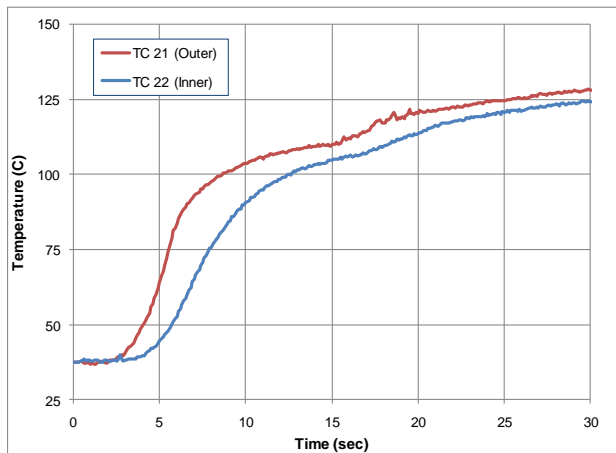


**Figure 14. TC 21/22 temperature data.**

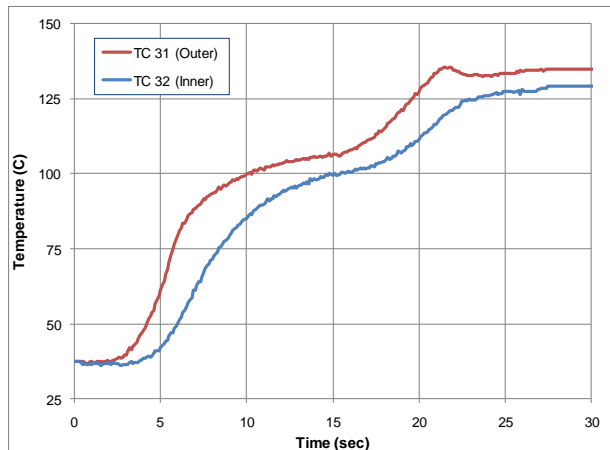


**Figure 15. TC 31/32 temperature data.**

The analysis required that we use the TC flight data to define the temperature boundary conditions over the entire vehicle model. However, the TCs on the conic section were not distributed along the full length of the cone (Fig. 12). The first TC on the cone (TC 4/3) was approximately 8 cm back from the forward edge and the last TC (TC 31/32) was approximately 5 cm forward of the aft end. In order to define a temperature history boundary condition over the entire cone existing TC data were both extrapolated and interpolated in order to define the temperature histories at the forward and aft ends of the cone. At the forward location the first two TCs on the cone were extrapolated linearly, with respect to the axial location, to the forward edge of the cone at each time step. At the aft location the last two TCs on the cone and the first two TCs on the cylindrical section were extrapolated linearly to the cone/cylinder interface, with respect to the axial location. Those two extrapolated values were then averaged to estimate the temperature at the cone/cylinder interface. An additional interpolated temperature point was added between the last TC on the cone and cone/cylinder interface, which was the average of last cone TC temperature and the interpolated temperature at the interface. Figure 16 shows an example of how the temperatures were estimated on the edges of the cone at 6 seconds into the flight. The measured TC temperatures on the cone, as a function of their axial location on the vehicle, are denoted by the solid circles. The estimated values at the forward edge of the cone, at axial location 0.2213 m, and the aft edge of the cone, at 1.1013 m, are shown as open circles. The temperature at the forward edge of the cone had to be extrapolated from the two TC because there were no surface TCs on the nose tip assembly from which the temperature could be interpolated. The forward end of the cone, made of aluminum, connects to the nose tip joiner, which was made of AISI 304 steel. We recognized that the extrapolated temperature and material property differences may result in a large error in estimated temperature at the forward end of the cone relative to the actual temperature response. The aft end of the cone is connected to the cylinder section, both of which are made of aluminum. The interpolated temperatures at that location should represent a relatively reasonable assumption.

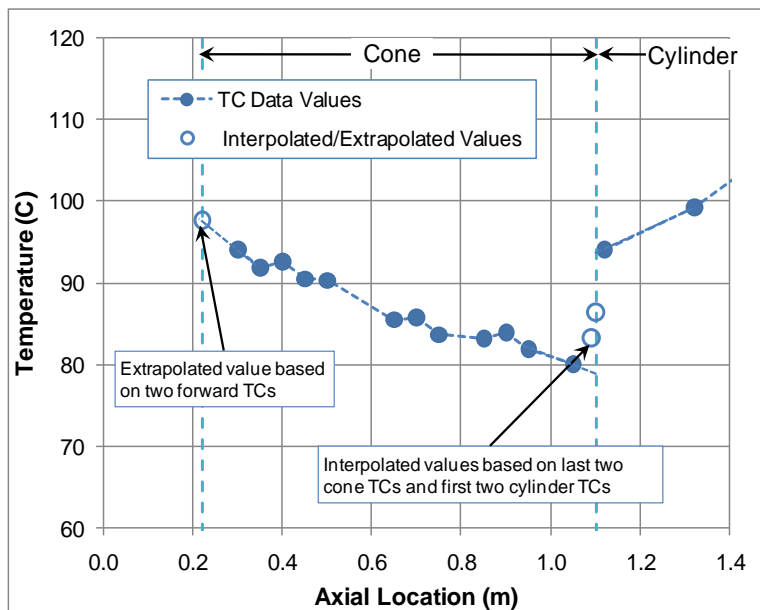


**Figure 16. Example of measured and estimated temperatures on the cone at 6.0 seconds.**

For the 2D analysis all of the good TC data on the 0° azimuthal ray of the cone was used to define the thermal boundary conditions. Figures 17 and 18 show the outer (surface) and inner (interior) temperature distributions from the TC data on the cone at several key times in the trajectory, respectively. The solid symbols represent actual TC data, while the open symbols represent the extrapolated or interpolated temperature values at the forward and aft end of the cone.

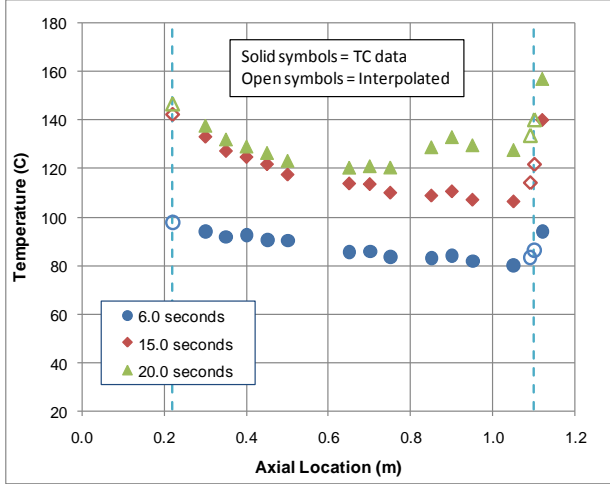


Figure 17. TC surface temperature distributions.

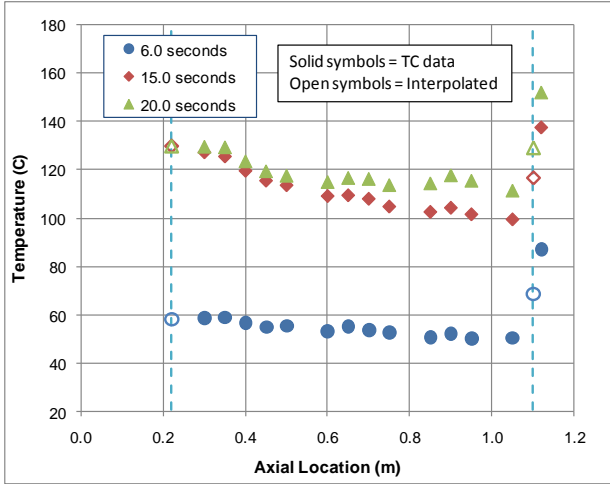


Figure 18. TC interior temperature distributions.

### E. Calculating Surface Heat Flux from Thermal Analysis

An inverse method was employed to calculate surface heat flux on the HIFiRE-1 vehicle based on the FE analysis results. A surface energy balance (Fig. 19) was used to relate the solid conduction into the structure for the FE analysis to the total aerothermal heat flux to the outer surface. The energy balance can be expressed in terms of Eq. 1. The quantities on the left side of the equation represent the components of the total heat flux to the surface,  $q_{total}$ . While the magnitude of the individual components of the total heat flux from the flight experiment cannot be deduced from just the thermocouple measurements, it is possible to estimate the values based on CFD analysis of the nominal flight conditions. In very severe hypersonic flight regimes, significant heating can occur from catalytic recombination of disassociate gas species at the wall ( $q_{cat}$ ) and from shock layer radiation ( $q_{rad\_in}$ ). The aerodynamic conditions for the ascent portion of the HIFiRE-1 flight, with a peak Mach number of 5.5, are not severe enough to produce significant catalytic or shock layer radiation heating. Virtually all of the sensible heating is the result of convection at the surface.

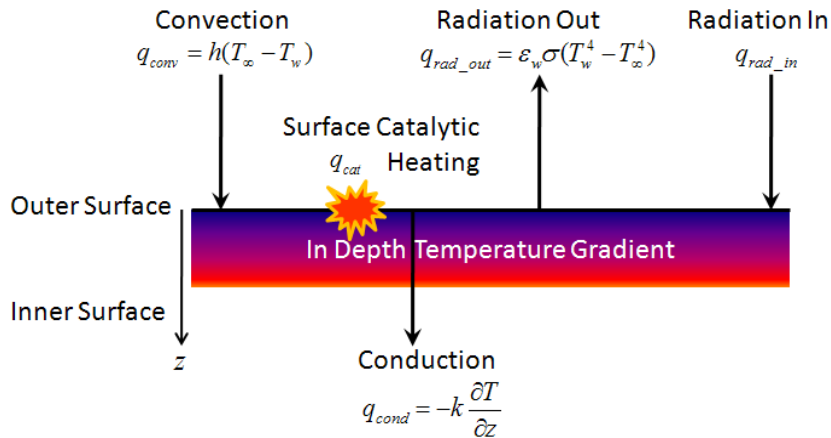


Figure 19. Surface energy balance.

$$\underbrace{q_{conv} + q_{rad\_in} + q_{cat}}_{total\ heat\ flux\ to\ the\ surface} = q_{cond} + q_{rad\_out} \quad (1)$$

The quantities on the right side of the equation can be determined independently. The finite element analysis is used to calculate the conduction heat flux into the surface,  $q_{cond}$ . The re-radiation from the surface,  $q_{rad\_out}$ , is calculated from the measured surface temperature,  $T_w$ , and the sink temperature,  $T_\infty$ , which was assumed to be 300K. We evaluated the magnitude of the re-radiation from the surface and found that, for the ascent portion of the trajectory, the surface temperature is still low enough on the conic section, below 150°C, that the radiation heat flux

is at least two orders of magnitude lower than the predicted convective heat flux. Therefore we assume that a good first order approximation of the total surface heat flux is equal to the conduction into the surface (Eq. 2).

$$q_{total} \approx q_{cond} \tag{2}$$

#### IV. Ground Test Data and CFD Predictions

An almost identical configuration to the HIFiRE-1 vehicle was tested at full scale in the LENS I shock tunnel facility at the CUBRC<sup>®</sup> Aerothermal/Aero-optic Evaluation Center (AAEC).<sup>7,8</sup> The LENS test configuration had a sharp nose tip, while the flight vehicle had a 2.5mm radius nose. Also, the flare section of the ground test vehicle was extended radially, so it had a slightly larger base diameter of 0.4092m versus the 0.355m flight vehicle. CFD predictions of both the ground test and flight experiment were performed using the Data-Parallel Line Relaxation (DPLR) tool.<sup>10</sup>

Comparison of the ground test data and CFD predictions on the conic section of the test vehicle were able to establish a boundary layer turbulent transition correlated to the momentum thickness Reynolds number ( $Re_\theta$ ). Figure 20 shows that at the axial location on the cone where turbulent transition occurred corresponded to  $Re_\theta = 653$ . CFD predictions of surface heat flux were also made for the flight conditions based on the nominal trajectory at 16 time points between 0 and 23.5 seconds, for both laminar and fully turbulent cases. The CFD analyses require an assumed constant wall temperature. All of the cases were run with a wall temperature value of 300K (27°C). At trajectory times greater than 15 seconds, a 400K (127°C) wall condition was also analyzed in order to assess the sensitivity of the predicted heat flux to the assumed wall temperature.

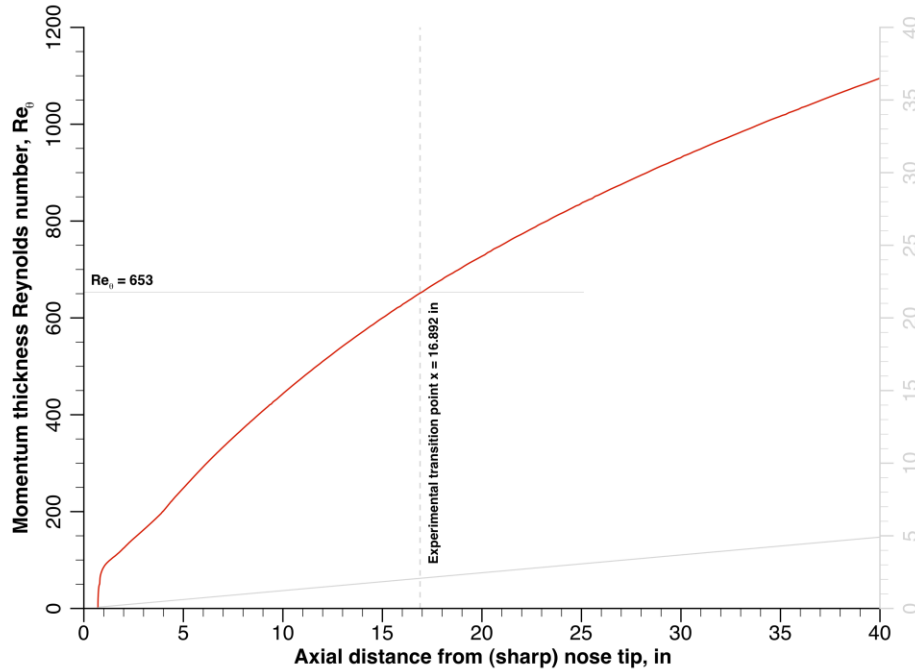


Figure 20. Turbulent transition criterion on conic section.

#### V. 1D Thermal Analysis Results

The predicted conduction heat flux history from the 1D FEA at the TC 31/32 location is shown in Figure 21. TC 31/32 is the farthest aft TC on the cone. The solid curves represent the results for both the prescribed inner surface (backface) temperature boundary condition and the adiabatic boundary condition. There is little difference between the two curves, suggesting that an adiabatic condition is a valid assumption in this case. The saw tooth nature of the curves reflects the noise in the temperature data. Both laminar and fully turbulent CFD cold wall heat flux predictions from DPLR are also shown on the figure. The turbulent heat flux values show remarkable correlation with the results from the thermal analysis over nearly the entire time until about 22 seconds, at which point the thermal analysis heat flux drops off dramatically. One explanation, that will be examined more carefully, is that the boundary layer, which is turbulent at that point on the cone for most of the ascent, is becoming laminar at about 22 seconds.

The same results for the TC 4/3 location, near the forward end of the cone, are shown in Figure 22. Here there is a noticeable difference in the heat flux predicted from the thermal analysis for the two different inner surface boundary conditions between 6 and 15 seconds, suggesting that the inner surface may not be completely adiabatic. The interior of the vehicle was filled with electronic equipment to support data acquisition and telemetry. It is possible that heat generated by that equipment is affecting the inner surface near the TC 4 location. We have not yet completely examined this possibility. The comparison with the turbulent CFD prediction shows good agreement until approximately 13 seconds. After 15 seconds the FEA predictions show very good agreement with the laminar CFD predictions. These results strongly suggest that, at the TC 4 location, the flow became laminar again around 15 seconds.

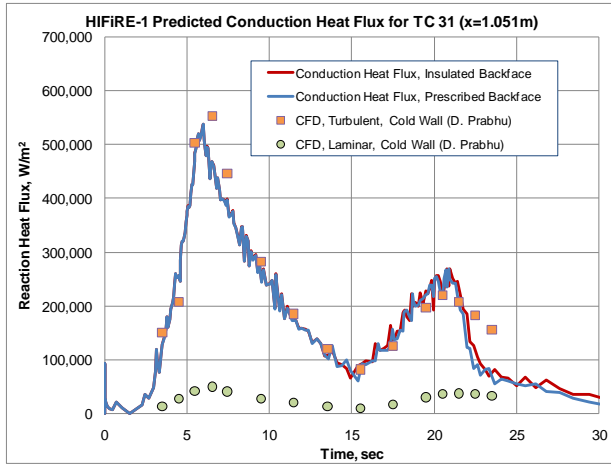


Figure 21. 1D analysis results for TC 31/32.

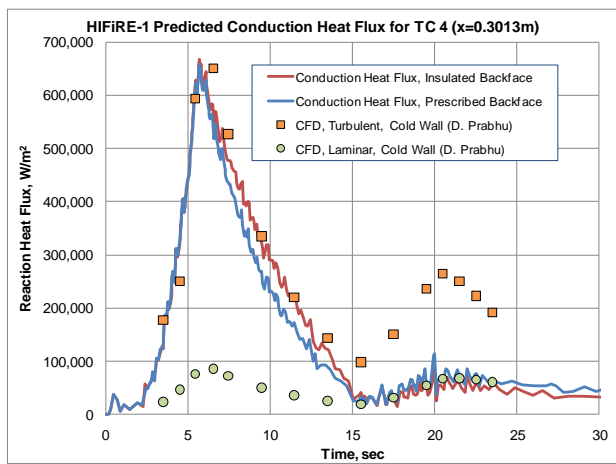


Figure 22. 1D analysis results for TC 4/3.

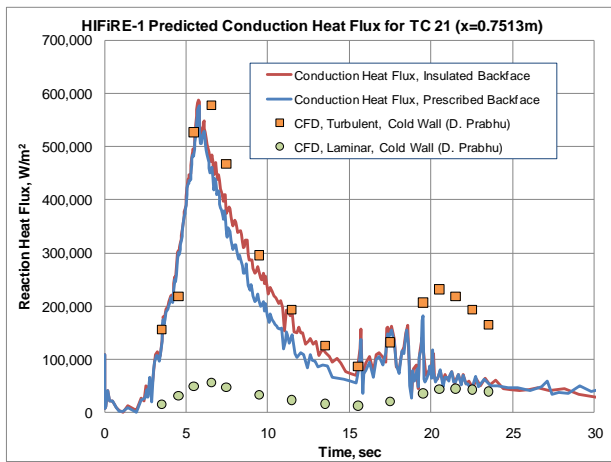


Figure 23. 1D analysis results for TC 21/22.

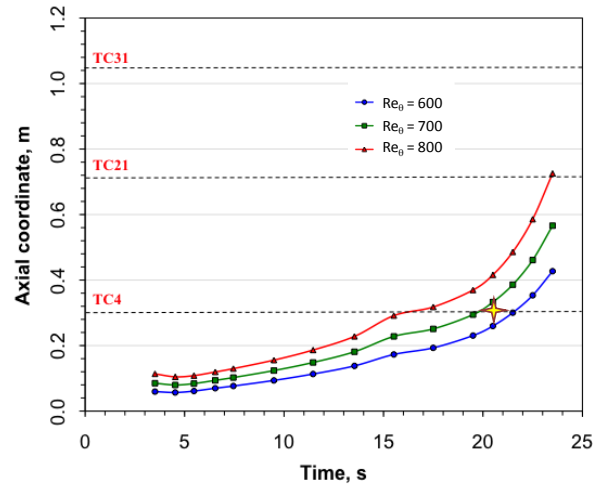


Figure 24. Turbulent transition criterion.

Figure 23 shows the results of the 1D FEA and CFD analyses at the TC 21/22 location, which is approximately in the middle of the cone section, halfway between TCs 43 and 31/32. The FEA results exhibit the same behavior between the two inner boundary condition cases as seen in the TC 4/3 results, which again may suggest some interaction with the inner surface and the internal electronics. The FEA predictions also show good agreement with the turbulent CFD predictions until about 17 seconds. Between 17 seconds and 22 seconds the FEA heat flux value oscillates between the laminar and turbulent CFD results. After 22 seconds the FEA heat flux agrees closely with the laminar CFD results.

An explanation of the behavior of the flight data may come from reexamining the turbulent transition criterion developed from the CFD predictions of the ground test data. Figure 24 shows the axial location of three specific momentum thickness Reynolds numbers as a function of trajectory time. The axial locations of the three TCs of interest are marked on the graph. CFD analysis of the ground test data predicted that the boundary layer would be turbulent at  $Re_{\theta} > 653$ . Based on that criterion, Figure 24 suggests that at the TC4 location, the boundary layer

should be turbulent up until about 21 seconds, which is where the TC4 axial location intersects a point between the  $Re_{\theta} = 600$  and  $Re_{\theta} = 700$  curves (marked by a yellow star).

The results in Figure 22 suggest that transition from turbulent back to laminar flow at the TC4 location occurs closer to 15 seconds, rather than 21 seconds at the  $Re_{\theta} > 655$  criterion would predict. At 15 seconds the results in Figure 24 indicate that  $Re_{\theta}$  is closer to 800 at the TC 4 location. If the transition criterion for flight is closer to  $Re_{\theta} = 800$ , then Figure 24 would predict that transition from turbulent back to laminar boundary layer flow should occur at the TC 21 location around 23 seconds, which is consistent with the results in Figure 23. An explanation of these results may be that for the flight conditions, the turbulence transition criterion is closer to  $Re_{\theta} = 800$  than  $Re_{\theta} = 650$ , as predicted from the shock tunnel experiments. A reason for this might be that the free stream flow conditions in the shock tunnel are noisier than the atmospheric conditions seen during the flight test, resulting in a transition to a turbulent boundary in the shock tunnel at a lower  $Re_{\theta}$  than during flight. The explanation will be examined more closely as this work progresses.

## VI. 2D Thermal Analysis Results

The evaluation of the 2D finite element analysis results had several objectives. The first objective was to assess the validity of the adiabatic inner wall boundary condition. The second was to assess any multi-dimensional conduction effects in the predicted surface heat flux. Finally, the 2D results would be compared with surface heat flux predictions from CFD analysis of the flight vehicle.

### A. Assessment of Adiabatic Inner Boundary Condition

The discussion of the 2D FEA results begins with a validation of the outer surface temperature boundary condition and an assessment of the inner surface thermal response. Figure 25 shows a comparison of the assigned TC temperature distribution at the surface (symbols) with the temperature distribution from the analysis (solid lines). The analysis results match exactly with the assigned temperatures, indicating that the boundary conditions were properly applied. Figure 26 shows a comparison of the inner surface TC temperature measurements (symbols) with the temperature distribution from the FE analysis case with the adiabatic inner surface condition (solid lines). If the inner surface of the flight vehicle was truly insulated, the analytical predictions of the inner surface temperature should match very closely to the measured values. At 6.0 seconds, there is a clear difference in the FEA predicted adiabatic inner wall temperatures and the measured values. The predicted temperatures are consistently lower than the measure values by as much as 8 degrees C. During the early ascent portion of the flight the noise in the TC data is about +/- 0.5 degrees C. So difference in the temperatures at 6.0 seconds may be due to some unaccounted energy source that is causing the interior surface of the cone to be warmer than it would if the surface was truly insulated. At times 15.0 and 20.0 seconds, however, the predicted inner surface temperatures match very closely to the measured values. This may suggest that the energy source that lead to the difference at 6.0 seconds was relatively small and transient.

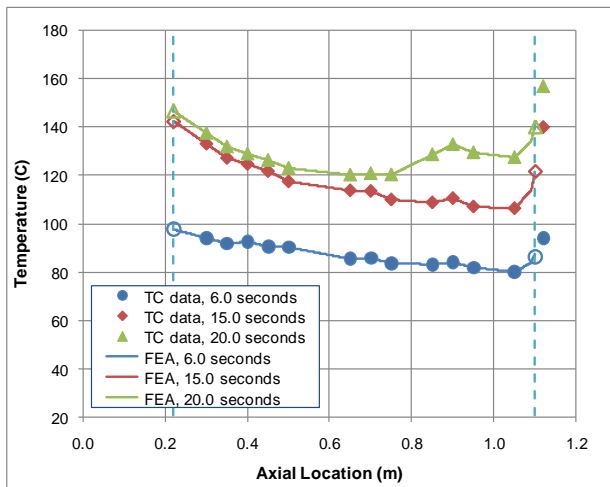


Figure 25. Outer surface temperatures results.

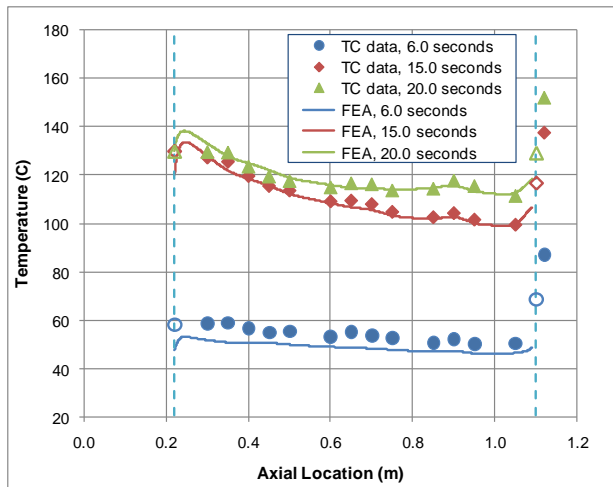


Figure 26. Inner surface temperature results.

The temperature histories at three TC locations are shown in Figures 27 through 29. In each case the 1D and 2D analysis at the inner surface with the adiabatic boundary condition are compared with the flight data. For the TC 3

(Fig. 27) and TC 22 (Fig. 28) the 1D and 2D predictions of the inner surface temperature history are nearly identical, indicating that the thermal response at those two locations is nearly one dimensional. That is, there are no significant multi-dimensional conduction effects, such as lateral conduction in the axial direction. In Figure 29 some difference in the temperatures between the 1D and 2D results can be seen, although the difference is on the order of 2 degrees C or less. In all cases the TC data shows a similar trend compared to the FEA predictions. Until about 5 seconds, the TC data matches very closely to the FEA results. Between 5 and 15 seconds the measured temperatures are slightly higher than those predicted by the adiabatic inner wall analysis, consistent with the results seen in Figure 26. The largest discrepancy occurs in the TC 3 data at 8 seconds, where the difference is about 12 degrees C. After 15 seconds the TC data tracks much closer to the analysis or just a bit lower. In Figure 29, for TC 31, which is located at the aft end of the cone, the temperatures appear to be diverging more noticeably with time. Overall the predicted inner surface temperatures matched the measured values closely enough that all subsequent 2D analyses, to predict surface heating, used the adiabatic inner surface boundary condition.

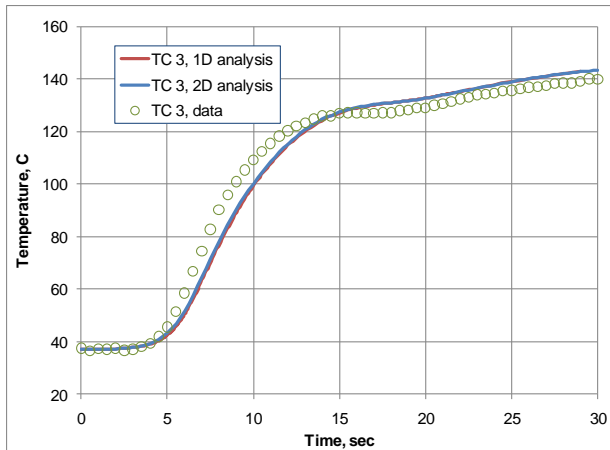


Figure 27. Temperature history results at TC 3.

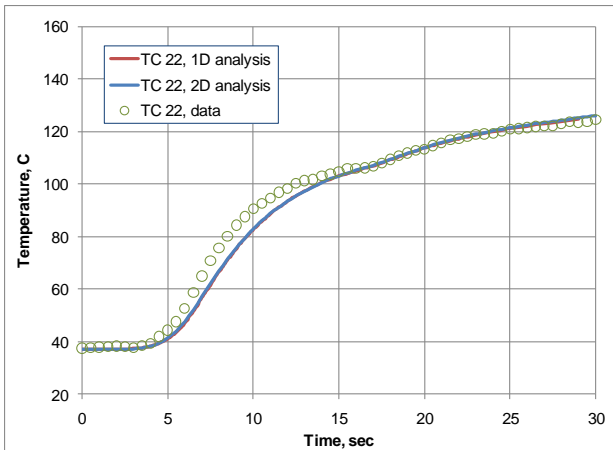


Figure 28. Temperature history results at TC 22.

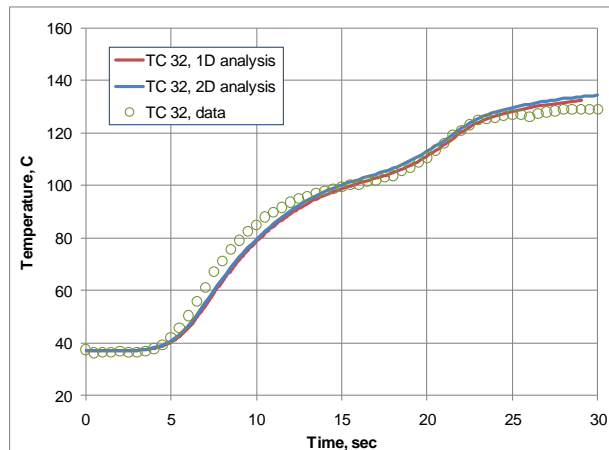
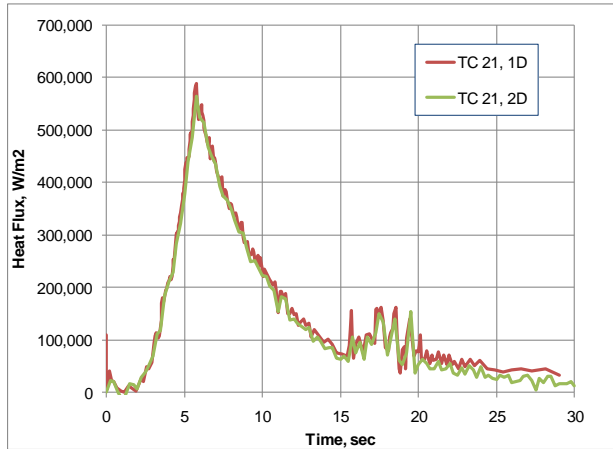
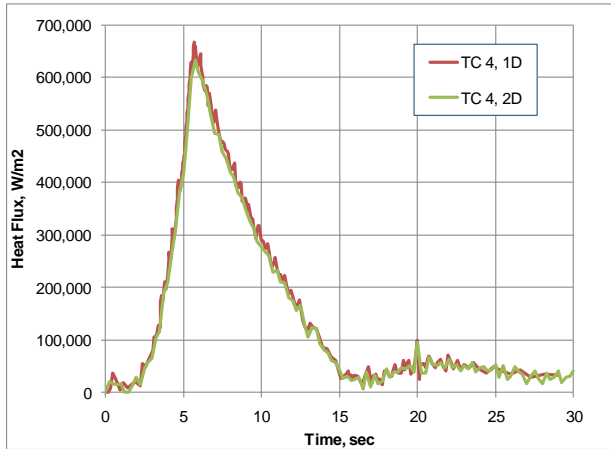


Figure 29. Temperature history results at TC 32.

### B. Assessment of 2D Conduction Effects

One of the objectives of the 2D analysis was to assess the magnitude of any multi-dimensional conduction effects in the thermal response of the vehicle structure. With the 2D axisymmetric FE model we can assess multi-dimensional conduction effects in the axisymmetric plane only. Any 3D, azimuthal conduction effects will be assessed in future 3D analyses. As noted in the preceding paragraph, the comparison of the 1D and 2D results for the temperature histories of the inner surface suggest that, at least for the two TC locations on the forward part of the cone, there were little or no 2D conduction effects. Figures 30 and 31 show a comparison of the heat flux history predictions for the 1D and 2D analyses at the locations of TC4 and TC21, respectively. The surface heat flux is based on an evaluation of Equation 2, where the internal conduction normal to the surface is extracted from the FEA

results. The good agreement between the two curves in each figure indicates that the thermal response through the cone structure is nearly 1D in nature, at least at the locations of the thermocouples.



**Figure 30. Comparison of 1D and 2D results at TC 4. Figure 31. Comparison of 1D and 2D results at TC 21.**

The heat flux history comparison for TC 31, the TC location furthest aft on the cone, is shown in Figure 32. After 6.0 seconds there is a clear difference between the predicted heat flux from the 1D and 2D analyses. The 2D heat flux is consistently lower than the value predicted by the 1D analysis. Physically this means that in order to maintain the same surface temperature at this location, which is prescribed by the boundary condition, the 2D model requires less input heat flux from the environment. This suggests that energy may be flowing laterally to this location from another part of the vehicle. In other words, there may be significant multi-dimensional conduction effects at this location.

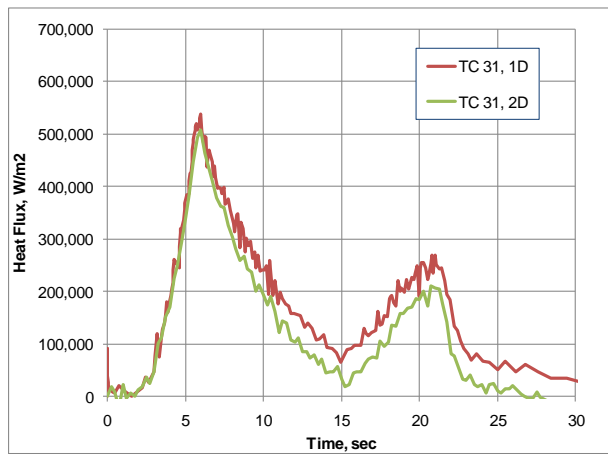


**Figure 32. Comparison of 1D and 2D results at TC 31.**

An examination of the vehicle region around TC 31 helps reveal the possible reasons for the difference between the 1D and 2D FEA heat flux results at that location. Figure 33 shows a detailed section of the interface between the aft of the cone section and the forward end of the cylinder section of the HIFiRE-1 vehicle FEA model. The locations of TC 31/32 on the cone and TC 107 on the cylinder are shown. These are the two TCs that define the temperature boundary condition at the interface between the sections. In addition to the large skin thickness difference between the cone (20 mm thick) and the cylinder (5 mm thick) there are some geometric features at the end of the cone which results in thickness variations.

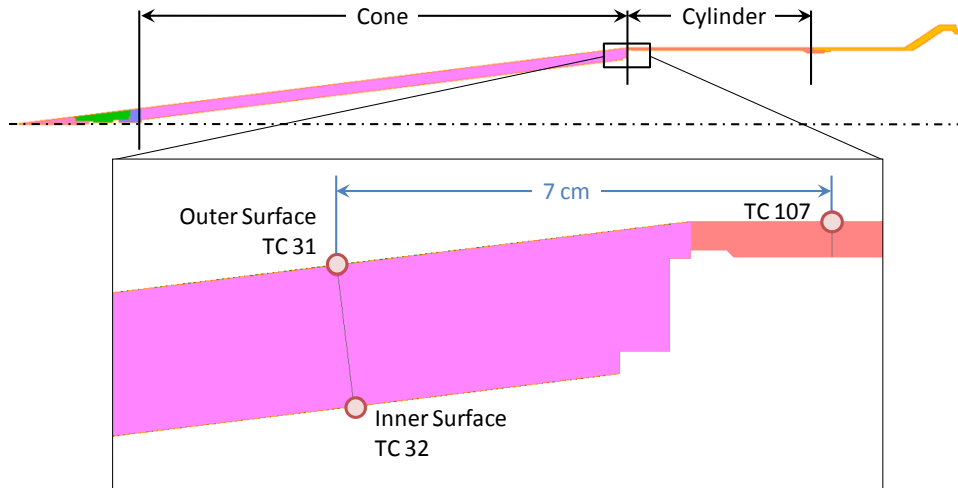


**Figure 33. Detail of the aft end of cone section.**

The geometry variations and the large change in measured surface temperatures between TCs 31 and 107 create large temperature gradients. Figures 34, 35, and 36 show the internal temperature contours in that region at 6.5, 15.5, and 20.5 seconds, respectively. At 6.5 seconds the temperature profile near TC 31 is nearly uniform along the length of the cone. Only near the interface with the cylinder does the profile begin to deviate from a uniform distribution. This is consistent with the flux time history shown in Figure 32 where the 1D and 2D flux predictions are nearly identical until about 6 seconds. Figure 35 shows the temperature contours at 15.5 seconds. At this time the temperature shows a significant gradient along the length of the cone and it seems that energy may be flowing from the hot cylindrical section into the cone section. Pre-flight CFD predictions show that the surface heat flux drops significantly as the flow passes the expansion corner at the interface between the cone and cylinder<sup>4</sup>. However, because the cylinder section is only 1/4<sup>th</sup> the thickness of the cone, there is less thermal mass to absorb energy and the surface temperature becomes higher than the cone section just forward of the junction. At 20.5 seconds (Fig. 36) there are still visible temperature gradients along the surface of the cone.

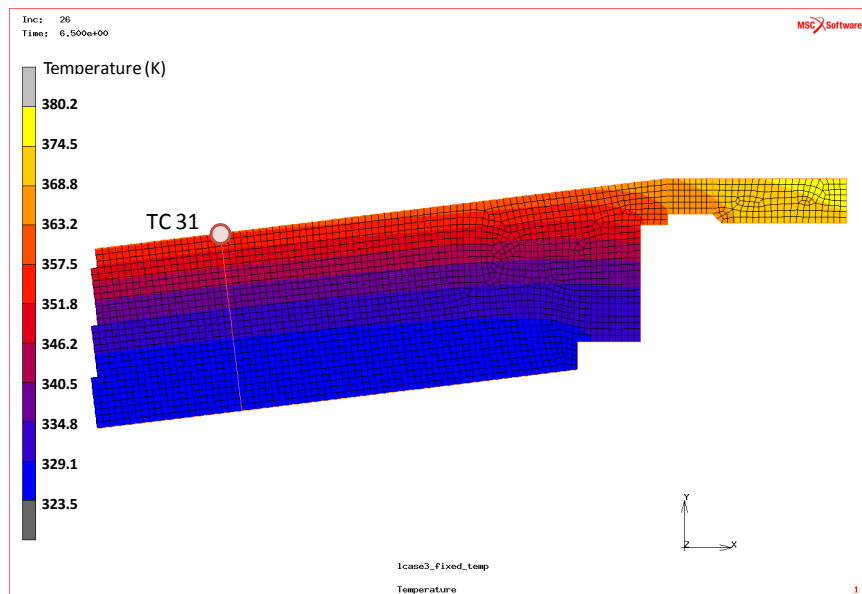


**Figure 34. Temperature contours at 6.5 seconds.**

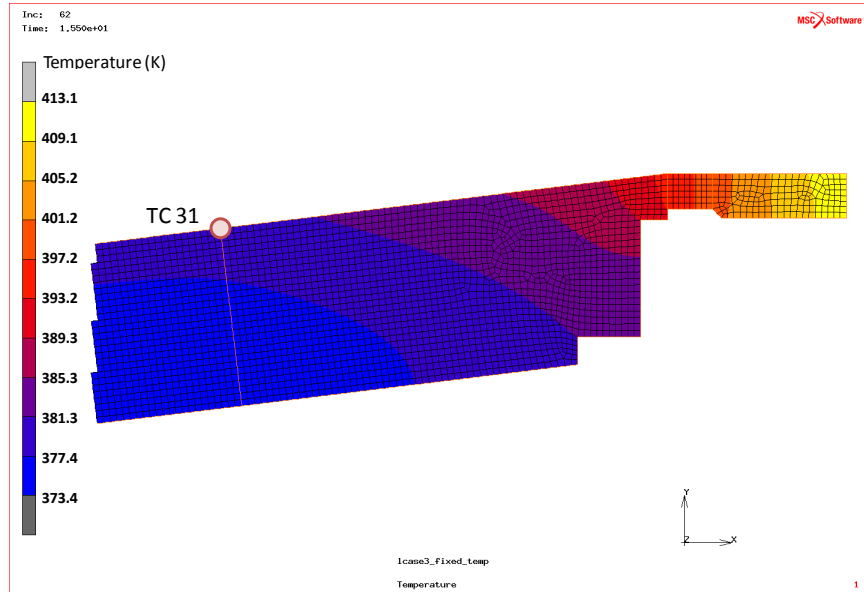


**Figure 35. Temperature contours at 15.5 seconds.**

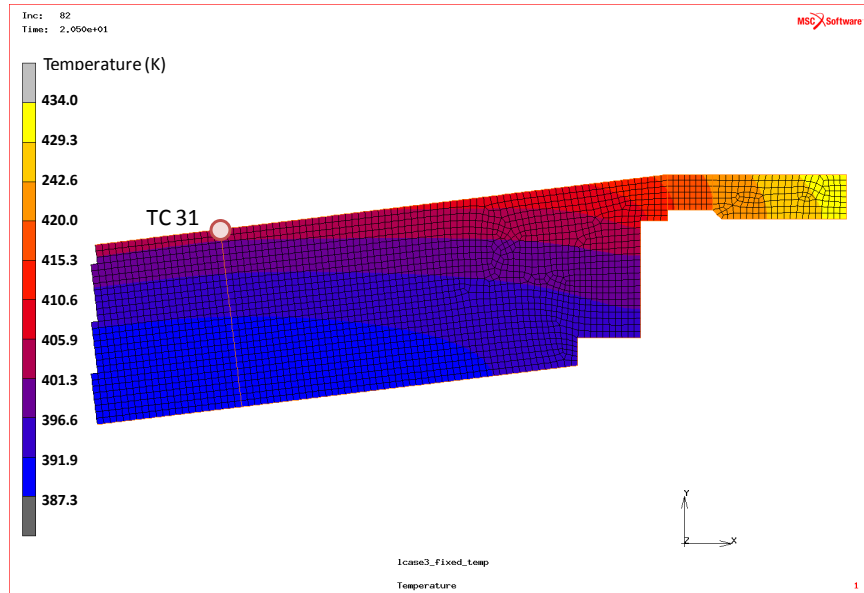


**Figure 36. Temperature contours at 20.5 seconds.**

The MSC.Marc post-processor, Mentat, has the option to view tensor data as a vector plot. The magnitude and direction of the heat flux can be visualized for these same trajectory times. Figures 37 through 39 show the heat flux vectors along the surface of the cone near the interface with the cylinder section. Note that each plot has a different heat flux scale. In Figure 37 the heat flux is nearly normal to the surface of the cone near the TC 31 location at 6.5 seconds. In the region around the interface between the cone and cylinder sections there is some indication of heat flow parallel to the surface, particularly along the inner surface. The magnitude of the heat flux is much lower at 15.5 seconds (Fig. 38) and while the majority of the energy is flowing normal to the surface of the cone, there is a noticeable component of heat flux parallel to the surface. The heat flux is again nearly normal to the surface at 20.5 seconds (Fig. 39), but there is clear evidence of energy flow from the cone/cylinder interface into the cone section.

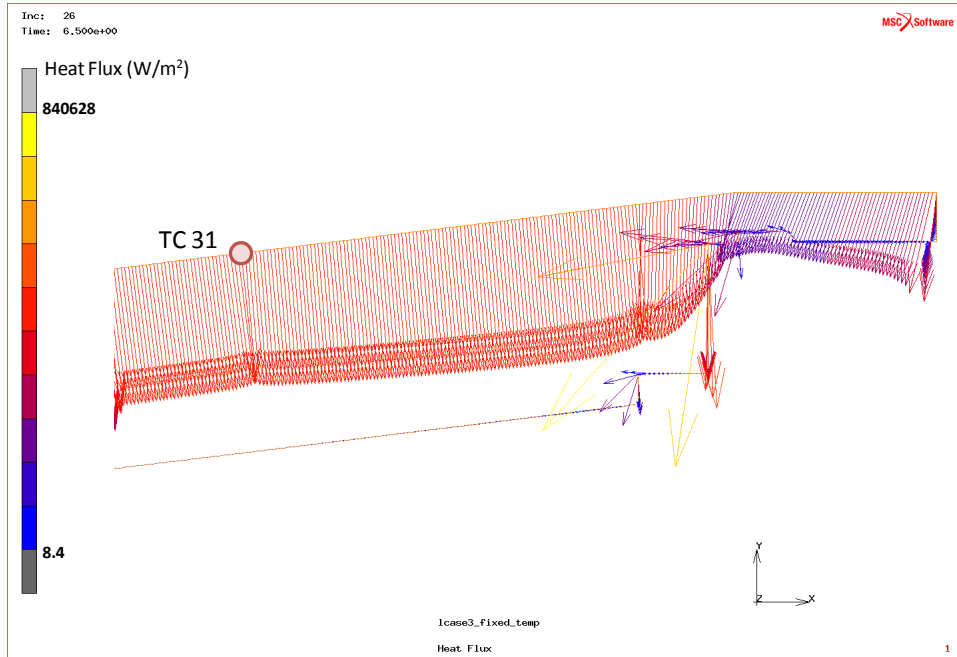


Figure 37. Heat flux vectors at 6.5 seconds.

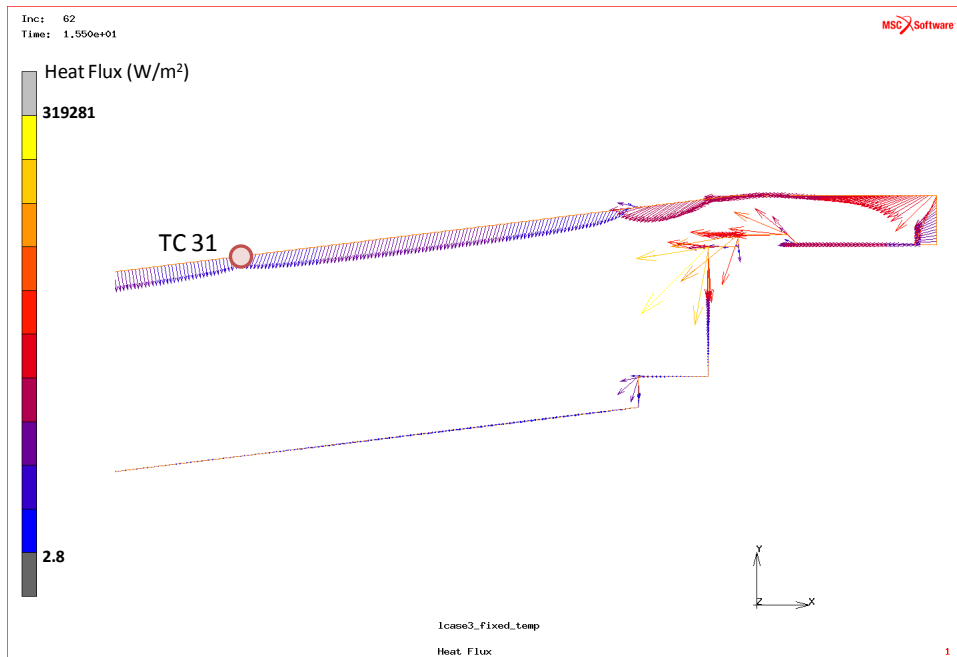
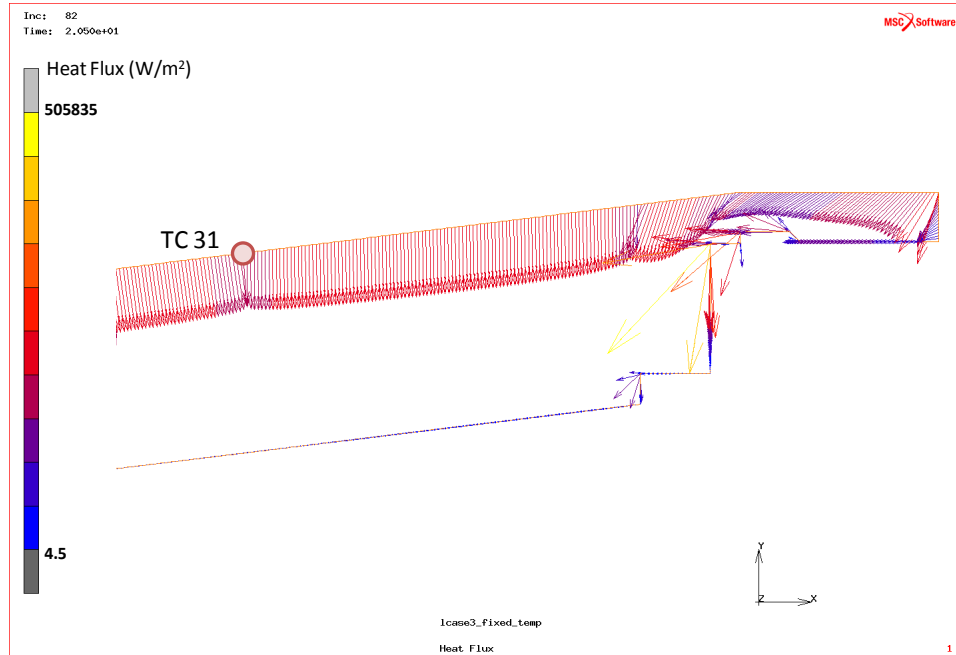


Figure 38. Heat flux vectors at 15.5 seconds.



**Figure 39. Heat flux vectors at 20.5 seconds.**

In all of the heat flux vector plots there is a noticeable inflection in the heat flux at the location of TC 31. The most reasonable explanation is that this represents an artifact of the way in which the temperature boundary condition was applied. The temperature history from the TC data is applied at the TC locations on the model. In between each TC, the temperature is linearly interpolated with streamlength. This guarantees a continuous surface temperature, but does not guarantee a continuous temperature derivative (slope) with respect to the streamlength. As a result, there is a discontinuity in the surface temperature gradient at each location on the model surface corresponding to a TC location. This discontinuity affects the heat flux prediction at that location and the result is the inflection that is visible in the vector plots. Note that the heat flux at the inflection point at the TC location is slightly lower than the surrounding surface heat flux in all cases. This may explain some of the discrepancy between the 1D and 2D predictions seen in Figure 32.

As our study continues we plan to use smooth curve fits of the surface temperature data as a boundary condition on the FEA model. We are currently investigating the appropriate curve fits to use. The difficulty is choosing the appropriate curve fitting algorithm is that we expect some variation in boundary layer flow conditions along the surface of the cone. In particular, there is evidence, that the flow becomes laminar again during the ascent and the transition from turbulent to laminar flow along with surface of the cone would be expected to produce at distinctive change in surface heat flux, which are reflected in the surface temperature measurements. Care must be taken in selecting curve fits of the surface temperature in order to maintain the effect of these flow features in the temperature profiles applied as boundary conditions in the FEA model. An inappropriate curve fit may unintentionally wash out these effects.

Based on the evaluation of the temperature contours and heat flux vector plots, it appear that the difference in heat flux predictions at the TC 31 location (Fig. 32) are probably the result of both real multi-dimensional conduction effects at the interface and unrealistic modeling artifacts as a result of the approach used to apply the temperature boundary condition. We intend to examine these effects in more detail as the study continues.

### C. Comparison of 2D FEA Results with CFD

One of the ultimate objectives of the HIFiRE program is to generate flight data to be used in verification of CFD models and tools. Figures 40 through 42 show the heat flux distributions at three trajectory times on the conic section of the HIFiRE-1 vehicle from the FEA predictions based on flight data and from laminar and turbulent CFD predictions from the DPLR program.<sup>10</sup> The analyses were based on the best estimated trajectory from the HIFiRE-1 flight. The CFD analyses were run in both fully laminar and fully turbulent modes, where the boundary layer was assumed to be either completely laminar or completely turbulent from the nose tip to the back of the cone. All of the cases were run with an assumed surface temperature of 300K (27°C). At trajectory times greater than 15 seconds, cases were also run with a 400K (127°C) wall temperature in order to assess the effect of wall temperature on the

estimated surface heat flux. The legends in the plots below indicate which wall temperature condition was used for the CFD results.

In all of the figures below, the FEA heat flux distributions show large changes in magnitude at the forward and aft ends of the conic section. As explained in the previous section, this behavior is probably the result of both real thermal effects at the interfaces between the vehicle sections and artifacts of the modeling approach used to apply the surface temperature boundary condition. There are also very obvious inflection points in the FEA heat flux distributions. These are the direct result of the temperature gradient discontinuity discussed in the previous section.

The FEA prediction of heat flux distribution on the cone at 6.5 seconds (Fig. 40) shows that it lies between the laminar and turbulent CFD prediction, although closer to the turbulent prediction. The trend in the FEA heat flux distribution is very similar to the turbulent CFD prediction, suggesting that the boundary layer was probably turbulent at that time. This is consistent with the transition criterion described in the previous section. At 15.5 seconds (Fig. 41) the FEA results near the forward part of the cone (left hand side of the curve) match closely to the laminar CFD prediction then shift closer to the turbulent prediction near the aft end. Again this is consistent with the CFD predictions of turbulence transition, which suggest that near 15 seconds the forward part of the conic section is likely to become laminar again. The heat flux distribution at 20.5 seconds shows an even more dramatic trend from laminar to turbulent behavior. Forward of the point at about 0.75 m the FEA prediction matches quite closely to the laminar CFD prediction. Aft of that point the FEA heat flux rapidly approaches the turbulent CFD values. In both the 15.5 and 20.5 second cases the FEA heat flux at the aft portion of the cone matches more closely to the CFD prediction based on the 300K wall condition than the 400K condition.

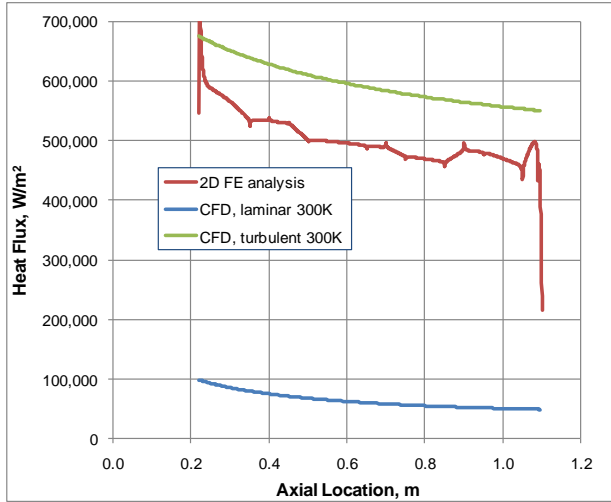


Figure 40. Heat flux distribution at 6.5 seconds.

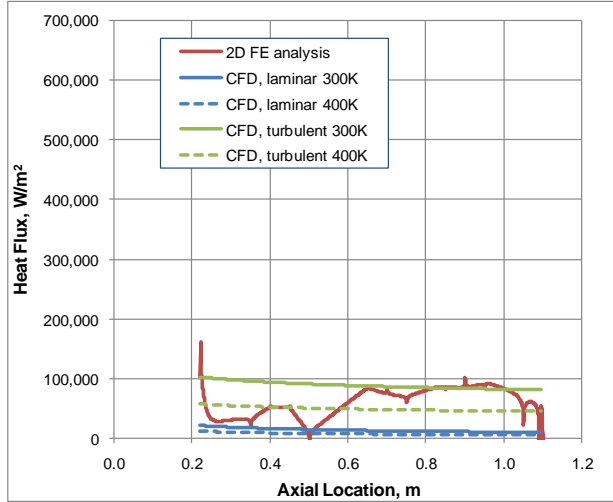


Figure 41. Heat flux distribution at 15.5 seconds.

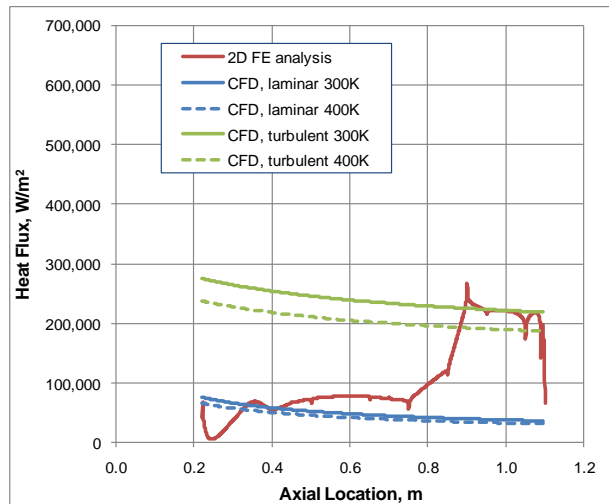


Figure 42. Heat flux distribution at 20.5 seconds.

## VII. Conclusions

We have used finite element thermal analysis of the HIFiRE-1 thermocouple data to estimate the surface heat flux on the vehicle during the flight test. The results of the analysis on the cone section of the vehicle show that, over most of the cone, the thermal response is essentially 1D through the thickness of the structure. Some 2D conduction effects may be present near the interfaces of the cone with the nose tip and the aft cylinder section. The FEA results also show that for most of the powered ascent portion of the flight, the interior surface of the cone behaves as if it were essentially adiabatic (insulated).

The FEA results are also very consistent with the CFD predictions for surface heat flux. Ground tests of a HIFiRE vehicle indicated that a momentum thickness Reynolds number ( $Re_\theta$ ) turbulent transition criterion was able to accurately define the transition state. The tests showed that for  $Re_\theta > 653$  the flow on the cone was turbulent. The analysis of the flight data indicates that the same type of transition criterion might be valid for the flight case, but that the actual value of  $Re_\theta$  maybe be closer to 800 for the flight conditions.

Evaluation of the FEA results also revealed some pitfalls in the analysis approach. The use of a piecewise linear surface temperature boundary condition lead to discontinuities in the surface temperature gradient, which in turn affected the predicted surface heat flux. These artifacts were clearly present in the heat flux distribution plots. As this study continues, we will examine the use of temperature boundary conditions that employ curve fits of the TC data. These curve fits should be continuous in both temperature and temperature gradient, while at the same time preserving any real effects of the boundary layer flow features, such as laminar/turbulent transition.

Further analysis of the HIFiRE-1 data is ongoing. In particular, the 2D FE analysis will be extended to include the entire vehicle cross section: cone, cylinder, and flare. The analysis will also be expanded to include the descent portion of trajectory. Eventually 3D FE analyses will be conducted to predict the azimuthal variation of heat flux due to geometry variations and non-zero angle-of-attack effects.

## Acknowledgments

This work was supported by the Hypersonics Project of the NASA Fundamental Aeronautics Program. The authors wish to thank the other HIFiRE-1 post-flight analysis team members for their support, including Meelan Choudhari (NASA Langley Research Center), David Adamczak (AFRL), Mark Smith (NASA Dryden Flight Research Center), Roger Kimmel (AFRL), and Deepak Bose (NASA Ames Research Center). Some of the work was performed under the Space Technology Research and Development (STRAD) contract, NASA contract number NNA10DE12C.

## References

1. Dolvin, D.J., "Hypersonic International Flight Research and Experimentation (HIFiRE) Fundamental Sciences and Technology Development Strategy," AIAA paper 2008-2581, *15th AIAA International Space Planes and Hypersonic Systems and Technologies Conference*, Dayton, OH, April 2008.
2. Adamczak, D., Alesi, H., Frost, M., "HIFiRE-1: Payload Design, Manufacture, Ground Test, and Lessons Learned," AIAA paper 2009-7294, October 2009.
3. Kimmek, R.L., "Aerothermal Design for the HIFiRE-1 Flight Vehicle," AIAA paper 2008-4024, *38th Fluid Dynamics Conference and Exhibit*, Seattle, WA, 23-26 June, 2008.
4. Adamczak, D., Kimmel, R.L., DSTO AVD Team, "HIFiRE-1 Flight Trajectory Estimation and Initial Experimental Results," AIAA paper 2011-2358, *17th AIAA International Space Planes and Hypersonic Systems and Technologies Conference*, San Francisco, CA, 11-14 April, 2011.
5. MacLean, M., Wadhams, T., Holden, M., and Johnson, H., "Ground Test Studies of the HIFiRE-1 Transition Experiment Part 2: Computational Analysis," *Journal Of Spacecraft And Rockets*, Vol. 45, No. 6, November–December 2008, pp. 1149-1164.
6. Kimmel, R.L., Adamczak, D., DSTO AVD Team, "HIFiRE-1 Preliminary Aerothermodynamic Measurements," AIAA paper 2011-3413, 41<sup>st</sup> AIAA Fluid Dynamics Conference, Honolulu, HI, 27-30 June, 2011.
7. Holden, M., MacLean, M., Wadhams, T., and Mundy, E., "Experimental Studies of Shock Wave/Turbulent Boundary Layer Interaction in High Reynolds Number Supersonic and Hypersonic Flows to Evaluate the Performance of CFD Codes," AIAA paper 2010-4468, *40th Fluid Dynamics Conference and Exhibit*, Chicago, IL 28 June - 1 July, 2010.
8. Wadhams, T., Mundy, E., MacLean, M., Holden, M., "Ground Test Studies of the HIFiRE-1 Transition Experiment Part 1: Experimental Results," *Journal of Spacecraft And Rockets*, Vol. 45, No. 6, November–December 2008, pp. 1134-1148.
9. MSC Software Corporation, Marc Version 2008r1, 2 MacArthur Place, Santa Ana, CA 92707.
10. Wright, M., Candler, G., and Bose, D., "Data-Parallel Line Relaxation Method for the Navier–Stokes Equations," *AIAA Journal*, Vol. 36, No. 9, 1998, pp. 1603–1609.